How the Fast Taylor-Fourier Transform (FTFT) will change the basic concepts of Power Systems?

José Antonio de la O Serna
Universidad Autónoma de Nuevo León
Monterrey, N. L., México

IEEE PES Big Data Tutorial Series
Virtual Event May 26, 2022

Outline

Introduction

- Fourier series and Discrete Forier transform (DFT) are very important to analyze *periodic* signal and sequences.

- A signal or a sequence is periodic if and only if: $x(t) = x(t + \ell T)$ or $x_n = x_{n+\ell N}$, respectively. Peridicity implies a horizontal structure or a periodic repetition.

- The mother signal of periodic signals is the Euler complex exponential function $e^{j2\pi k F_1 t}$, or the sequence $e^{j\frac{2\pi}{N}kn}$.

- One of the basic concepts of power systems is the phasor, a complex number providing amplitude and phase angle of a steady-state sinusoidal signal.

- Fourier series can be applied without error when the power system is in *steady-state*.

- When the power system is under dynamic conditions, it is better to apply the Laplace or the Prony theory.

Fourier Equations

The synthesis and analysis equations of the Fourier series:

$$x(t) = \sum_{h=-\infty}^{\infty} c_h e^{j2\pi h F_1 t}, t \in [-\frac{T_1}{2}, \frac{T_1}{2}), \quad c_h = \frac{1}{T_1} \int_0^{T_1} x(t) e^{-j2\pi h F_1 t}. \tag{1}$$

The Discrete time version, for N samples per fundamental period:

$$x_n = \sum_{k=0}^{N-1} \tilde{c}_h e^{j\frac{2\pi}{N} hn}, n = 0, 1, \ldots, N-1 \quad \tilde{c}_h = \frac{1}{N} \sum_{n=0}^{N-1} x_n e^{-j\frac{2\pi}{N} hn}. \tag{2}$$

and the *DFT* (or *FFT*) in matrix form:

$$x = \frac{1}{N} W_N \xi, \qquad x \in \mathcal{R}^N, \xi \in \mathcal{C}^N, \qquad \xi = W_N^H x, \tilde{c} = \frac{1}{N} \xi. \tag{3}$$

Research Problem: Power Oscillations

Periodicity is lost in oscillatory conditions:
Amplitude and phase angle modulated sinusoidal signal
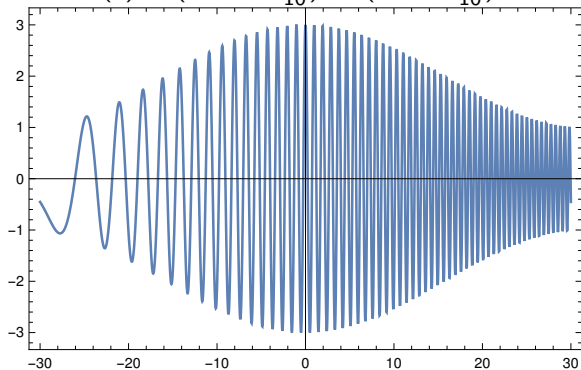$$s(t) = (2 + \cos\tfrac{t}{10})\cos(2\pi t + \tfrac{t^2}{10}).$$

Figure 1: Oscillatory signal, time in cycles. Amplitude and phase angle modulated signal.

Triangular Oscillatory Signal

- Harmonics are amplitude and phase modulated when a periodic signal oscillates.
- Their linear spectre widens by the complex envelope of the oscillation which acts as a window function over the full set of harmonic frequencies.
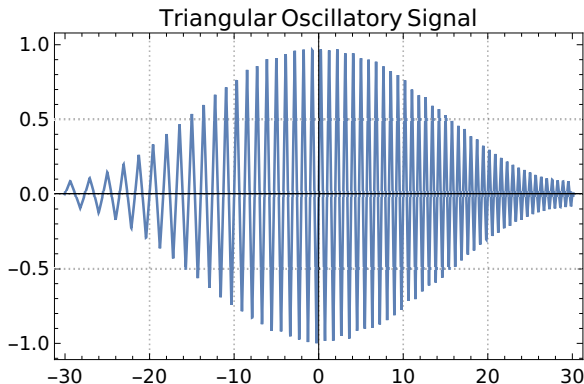

Figure 2: Triangular oscillatory signal, time in cycles.

Taylor-Fourier Signal Model

The complete response of a linear system due to a singularity of multiplicity $K + 1$ at $s_h = -\sigma_h + j\omega_h$ is of the form:

$$x(t) = \underbrace{(c_K t^K + c_{K-1} t^{K-1} + \ldots + c_0) \, e^{-\sigma_h t} \, \underbrace{\underbrace{e^{j\omega_h t}}_{Fourier}}_{Prony}}_{Taylor-Fourier}$$

which corresponds to $Res\{H(s)e^{st}\}|_{s_h}$.

- **Fourier** signal model is the poorest one, since it assumes single singularities at harmonic frequencies: $c_h e^{jh\omega_1 t}, h \in \mathcal{Z}$.
- **Prony** signal model adds attenuation to the former one: $c_h e^{-\sigma_h t} e^{j\omega_h t}$.
- **Taylor-Fourier** signal model is the most complete, since it assumes repeated singularities: $(c_K t^K + c_{K-1} t^{K-1} + \ldots + c_0)e^{-\sigma_h t} e^{j\omega_h t}$

TFT Signal Model

Signal model of TFT is:

$$x(t) = \sum_{h=-\infty}^{\infty} \xi_h(t) e^{j2\pi h f_1 t}, \qquad -C\frac{T_1}{2} \leq t \leq C\frac{T_1}{2}. \quad (4)$$

where $\xi_h(t) \in \mathbb{C}$ is the *h*-th *complex envelope or dynamic phasor*, that replace the static *Fourier coefficient* of DFT. Each one of these functions are approached by a *K*-th Taylor expansion of the form

$$\xi_h^{(K)}(t) = \xi_h(t_0) + \dot{\xi}_h(t_0)t + \cdots + \overset{(K)}{\xi}_h(t_0)\frac{t^K}{K!} \quad (5)$$

where the coefficients $\overset{(k)}{\xi}_h(t_0) \in \mathbb{C}$ are the *k*-th derivatives of complex envelope $\xi_h(t)$, corresponding to the *h*-th harmonic frequency in (4). The time evolution of these coefficients perform as *state spectrograms* of $x(t)$.

$$x_K = \Phi_K \xi_K = \left(I \begin{pmatrix} W_N \\ W_N \\ \vdots \\ W_N \end{pmatrix} \quad T \begin{pmatrix} W_N \\ W_N \\ \vdots \\ W_N \end{pmatrix} \quad \cdots \quad \frac{1}{K!} T^K \begin{pmatrix} W_N \\ W_N \\ \vdots \\ W_N \end{pmatrix} \right) \begin{pmatrix} \xi_N \\ \dot{\xi}_N \\ \vdots \\ \overset{(K)}{\xi}_N \end{pmatrix}$$ (6)

For $K = 1$:

$$x_1 = \Phi_1 \xi_1 = \left(I \begin{pmatrix} W_N \\ W_N \end{pmatrix} \quad T \begin{pmatrix} W_N \\ W_N \end{pmatrix} \right) \begin{pmatrix} \xi_1 \\ \dot{\xi}_1 \end{pmatrix}$$

And for $K = 3$:

$$x_3 = \Phi_3 \xi_3 = \left(I \begin{pmatrix} W_N \\ W_N \\ W_N \\ W_N \end{pmatrix} \quad T \begin{pmatrix} W_N \\ W_N \\ W_N \\ W_N \end{pmatrix} \quad \frac{T^2}{2} \begin{pmatrix} W_N \\ W_N \\ W_N \\ W_N \end{pmatrix} \quad \frac{T^3}{6} \begin{pmatrix} W_N \\ W_N \\ W_N \\ W_N \end{pmatrix} \right) \begin{pmatrix} \xi_3 \\ \dot{\xi}_3 \\ \ddot{\xi}_3 \\ \dddot{\xi}_3 \end{pmatrix}$$
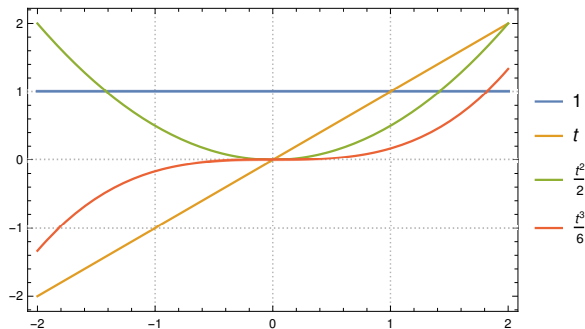
Figure 3: Taylor terms for $K = 3$.

Solution: Analysis Equation

The Taylor-Fourier transform is given by the analysis equation:

$$\xi_K = \Phi_K^{-1} x_K \qquad (7)$$

If $\widetilde{\Phi}_K$ is the dual matrix of Φ_K:

$$\widetilde{\Phi}_K = (\Phi_K^{-1})^H \qquad (8)$$

$\widetilde{\Phi}_K$ and Φ are biorthogonal, since $\widetilde{\Phi}_K^H \Phi = I$.

Factorization into Taylor and Fourier Operators

$$\Phi_K = \Upsilon_K \Omega_K$$

$$= \begin{pmatrix} I & T_1 & \dots & \frac{1}{K!}T_1^K \\ I & T_2 & \dots & \frac{1}{K!}T_2^K \\ \vdots & \vdots & \ddots & \vdots \\ I & T_C & \dots & \frac{1}{K!}T_C^K \end{pmatrix} \begin{pmatrix} W_N & 0 & \dots & 0 \\ 0 & W_N & \dots & 0 \\ \vdots & \vdots & \ddots & \vdots \\ 0 & 0 & \dots & W_N \end{pmatrix} \qquad (9)$$

where $C = K + 1$ and T_c are $N \times N$ diagonal submatrices with consecutive cyclic pieces of the Kth Taylor term.

We have

$$\Phi_K^{-1} = \Omega_K^{-1} \Upsilon_K^{-1} = \frac{\Omega_N^H}{N} \widetilde{\Upsilon}_K^T \qquad (10)$$

In consequence the dual of the Taylor operator is given by:

$$\widetilde{\Upsilon} = \frac{Cof(\Upsilon)}{|\Upsilon|}. \qquad (11)$$

Key Idea for the Solution ($K = 1$)

For $K = 1$, $t_1 = t_{[-T_1, 0)}$, and $t_2 = t_{[0, T_1)} = t_1 + T_1$, we have

$$\Upsilon_1 = \begin{pmatrix} 1 & t_1 \\ 1 & t_2 \end{pmatrix} \tag{12}$$

with $|\Upsilon_1| = t_2 - t_1 = T_1$. Then, we have:

$$\widetilde{\Upsilon}_1 = \frac{\begin{pmatrix} t_2 & -1 \\ -t_1 & 1 \end{pmatrix}}{T_1} = \begin{pmatrix} u_1 + 1 & -F_1 \\ -(u_2 - 1) & +F_1 \end{pmatrix} \tag{13}$$

where u_n is the normalized time: $u = t_n / T_1$. Its first column is a triangular pulse:

$$\widetilde{v}_1^{(1)}(u) = \begin{cases} u + 1 & \text{for} \quad -1 \le u < 0, \\ 1 - u & \text{for} \quad 0 \le u < 1, \\ 0 & \text{otherwise,} \end{cases} \tag{14}$$

and the second one is a scaled Haar wavelet: $\widetilde{v}_2^{(1)}(u) = -F_1 \dot{\widetilde{v}}_1(u)$.

Key idea for the solution ($K = 2$)

For $K = 2$, we have

$$\Upsilon_2 = \begin{pmatrix} 1 & t_1 & t_1^2/2 \\ 1 & t_2 & t_2^2/2 \\ 1 & t_3 & t_3^2/2 \end{pmatrix}. \tag{15}$$

with $t_1 = t_{[-\frac{3T_1}{2}, \ -\frac{T_1}{2})}$, $t_2 = t_1 + T_1$, and $t_3 = t_1 + 2T_1$. In this case $|\Upsilon_2| = T_1^3$, and

$$\widetilde{\Upsilon}_2 = \begin{pmatrix} \frac{1}{2}(u_1 + 2)(u_1 + 1) & -F_1(u_1 + \frac{3}{2}) & F_1^2 \\ -(u_2 + 1)(u_2 - 1) & 2F_1 u_2 & -2F_1^2 \\ \frac{1}{2}(u_3 - 1)(u_3 - 2) & -F_1(u_3 - \frac{3}{2}) & F_1^2 \end{pmatrix}. \tag{16}$$
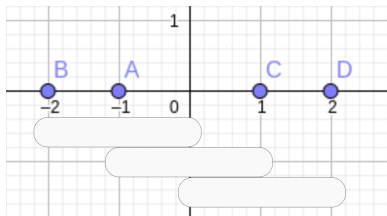
Key Idea ($K = 3$)

Finally, for $K = 3$, $t_1 = t_{[-2T_1, -T_1)}$ and $t_n = t_1 + (n-1)T_1$ $n = 2, 3, 4$.
We have $|\Upsilon_3| = T_1^6$. Its first dual column is:

$$\widetilde{v}_1^{(3)}(u) = \begin{cases} \frac{1}{6}(u+3)(u+2)(u+1) & \text{for } -2 \leq u < -1, \\ -\frac{1}{2}(u+2)(u+1)(u-1) & \text{for } -1 \leq u < 0, \\ \frac{1}{2}(u+1)(u-1)(u-2) & \text{for } 0 \leq u < 1, \\ -\frac{1}{6}(u-1)(u-2)(u-3) & \text{for } 1 \leq u < 2, \\ 0 & \text{otherwise.} \end{cases} \qquad (17)$$

and the following ones are: $\widetilde{v}_2^{(3)}(u) = -F_1 \dot{\widetilde{v}}_1^{(3)}(u), \widetilde{v}_3^{(3)}(u) = F_1^2 \ddot{\widetilde{v}}_1^{(3)}(u),$
and $\widetilde{v}_4^{(3)}(u) = (-F_1)^3 \dddot{\widetilde{\varphi}}_0^{(3)}(u).$
O-splines are recognized as the *Lagrange central interpolation kernels*.

O-splines and derivatives up to $K = 3$.

.
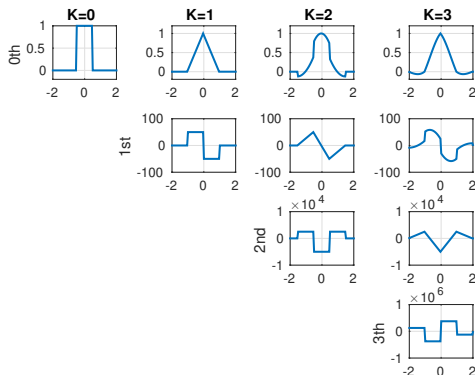
Figure 5: At the top, the O-splines of order K, for $K = 0, 1, 2, 3$, below each one of them its successive derivatives.

O-splines are stable functions or Multiresolution Analysis (MRA) *generators*

If $\varphi(u) \in V_0$, the set of integer translates $\{\varphi(u-n)\}_{n \in \mathcal{Z}}$ is an *inconditional basis* (or Riesz basis) of V_0, and forms a Multiresolution Analysis on $\mathcal{R}$.

O-Splines

- Splines are polynomial piecewise functions used normally in interpolation.
- O-splines[1] are used for implementing the Taylor-Fourier transform.
- Odd order O-splines are cardinal splines: continuous functions of compact support with zero crossings at their knots.
- They are used here as bandpass filters to analyze oscillations.
- They converge to the ideal filter as the order $K \to \infty$.
- In interpolation, odd order O-splines correspond with the Lagrange central interpolation kernel of the same order.

---

[1] J. A. de la O Serna, "Dynamic Harmonic Analysis with FIR filters designed with O-splines", *IEEE Transactions on Circuits and Systems I: Regular Papers*, Vol.67, No.12, Dec. 2020, pp. 5092-5100.

O-splines II

- O-splines in closed-form reduce the computational complexity of the DTTFT.
- In addition, each O-spline comes with its derivatives, which perform as ideal differentiators.
- They provide a sequence of adjustable FIR filters that offer optimal coefficients for Hermite interpolation of the approximated function.
- They are very useful for multi-resolution and time-frequency analysis.
- A new family of wavelets build with linear combinations of O-splines is coming soon.

O-splines Relationships

$$\varphi^0(u) = \begin{cases} 1 & \text{for } -\frac{1}{2} \le u \le \frac{1}{2} \\ 0 & \text{otherwise} \end{cases} \tag{18}$$

The first O-spline

$$\varphi^1(u) = \begin{cases} u + 1 & \text{for } -1 \le u \le 0 \\ -(u - 1) & \text{for } 0 \le u \le 1 \\ 0 & \text{otherwise} \end{cases} \tag{19}$$

and its first derivative:

$$\dot{\varphi}^1(u) = f_0(\varphi^0(u + \frac{1}{2}) - \varphi^0(u - \frac{1}{2})) \tag{20}$$

O-splines Relationships

The second O-spline

$$\varphi^2(u) = \begin{cases} \frac{1}{2}(u+2)(u+1) & \text{for } -\frac{3}{2} \leq u \leq -\frac{1}{2} \\ -(u+1)(u-1) & \text{for } -\frac{1}{2} \leq u \leq \frac{1}{2} \\ \frac{1}{2}(u-1)(u-2) & \text{for } \frac{1}{2} \leq u \leq \frac{3}{2} \\ 0 & \text{otherwise,} \end{cases} \tag{21}$$

its first derivative:

$$\dot{\varphi}^2(u) = f_0(\varphi^1(u+\frac{1}{2}) - \varphi^1(u-\frac{1}{2})), \tag{22}$$

and its second derivative:

$$\ddot{\varphi}^2(u) = f_0^2(\varphi^0(u+1) - 2\varphi^0(u) + \varphi^0(u-1)). \tag{23}$$

O-splines Relationships

And finally the third O-spline:

$$\varphi^3(u) = \begin{cases} \frac{1}{6}(u+3)(u+2)(u+1) & \text{for } -2 \leq u \leq -1 \\ -\frac{1}{2}(u+2)(u+1)(u-1) & \text{for } -1 \leq u \leq 0 \\ \frac{1}{2}(u+1)(u-1)(u-2) & \text{for } 0 \leq u \leq 1 \\ -\frac{1}{6}(u-1)(u-2)(u-3) & \text{for } 1 \leq u \leq 2 \\ 0 & \text{otherwise,} \end{cases} \tag{24}$$

its first derivative:

$$\dot{\varphi}^3(u) = f_0(\varphi^2(u+\frac{1}{2}) - \varphi^2(u-\frac{1}{2})), \tag{25}$$

its second derivative:

$$\ddot{\varphi}^3(u) = f_0^2(\varphi^1(u+1) - 2\varphi^1(u) + \varphi^1(u-1)) \tag{26}$$

and, finally its third derivative:

$$\dddot{\varphi}^3(u) = f_0^3(\varphi^0(u+\frac{3}{2}) - 3\varphi^0(u+\frac{1}{2}) + 3\varphi^0(u-\frac{1}{2}) - \varphi^0(u-\frac{3}{2})) \tag{27}$$

101st O-spline
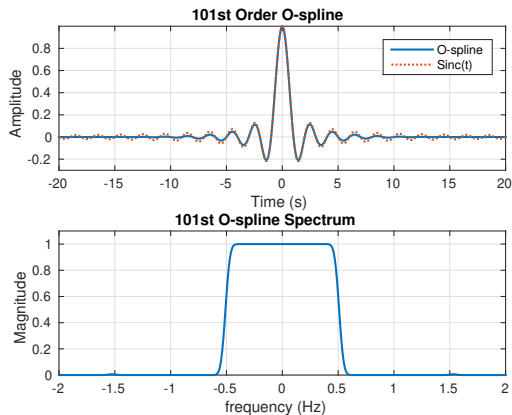
Figure 6: O-spline $K = 101$

For $h = 0$:

$$
\begin{aligned}
a_0(t_0) &= \xi_0(t_0), & \varphi_0(t_0) &= 0, \\
\dot{a}_0(t_0) &= \dot{\xi}_0(t_0), & \dot{\varphi}_0(t_0) &= 0, \\
\ddot{a}_0(t_0) &= \ddot{\xi}_0(t_0) & \ddot{\varphi}_0(t_0) &= 0.
\end{aligned}
\tag{28}
$$

and for $h > 0$:

$$
\begin{aligned}
a_h(t_0) &= 2|\xi_h(t_0)|, \\
\varphi_h(t_0) &= \angle \xi_h(t_0), \\
\dot{a}_h(t_0) &= 2\mathrm{Re}\{\dot{\xi}_h(t_0)e^{-j\varphi_h(t_0)}\}, \\
\dot{\varphi}_h(t_0) &= \frac{2}{a_h(t_0)}\mathrm{Im}\{\dot{\xi}_h(t_0)e^{-j\varphi_h(t_0)}\}, \\
\ddot{a}_h(t_0) &= 2\mathrm{Re}\{\ddot{\xi}_h(t_0)e^{-j\varphi_h(t_0)}\} + a_h(t_0)\dot{\varphi}_h(t_0)^2, \\
\ddot{\varphi}_0(t_0) &= \frac{\mathrm{Im}\{\ddot{\xi}_h(t_0)e^{-j\varphi_h(t_0)}\} - 2\dot{a}_h(t_0)\dot{\varphi}_h(t_0)}{a_h(t_0)}.
\end{aligned}
\tag{29}
$$

Nonic O-spline Spectrogram of $s(t) = cos(120\pi t + \varphi(t))$

with $\varphi(t) = e^{-4t}\cos(10\pi t)$, and

$\dot{\varphi}(t) = -4e^{-4t}\cos(10\pi t) - 10\pi e^{-4t}\sin(10\pi t)$
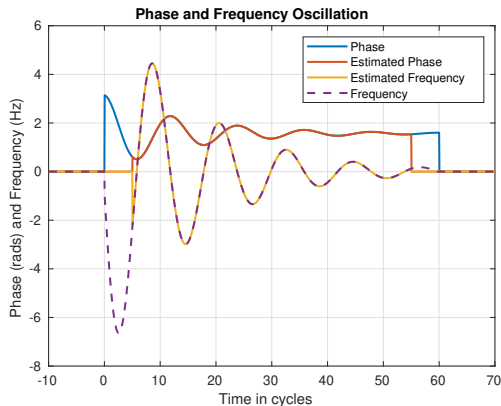
Figure 7: Nonic O-spline Spectogram of $s(t)$.

O-splines for $K = 1, ..., 11$
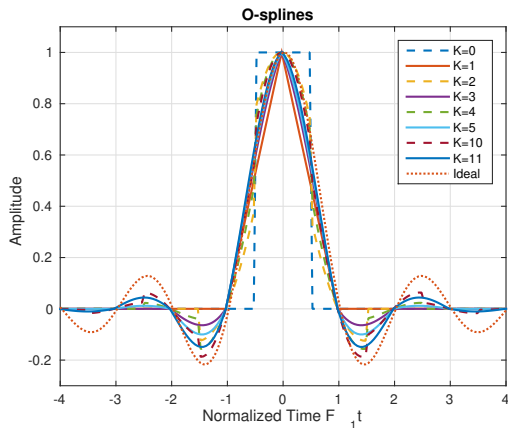
Figure 8: O-splines for $K = 0, 1, \ldots, 5, 10$ and 11.

O-spline Spectra
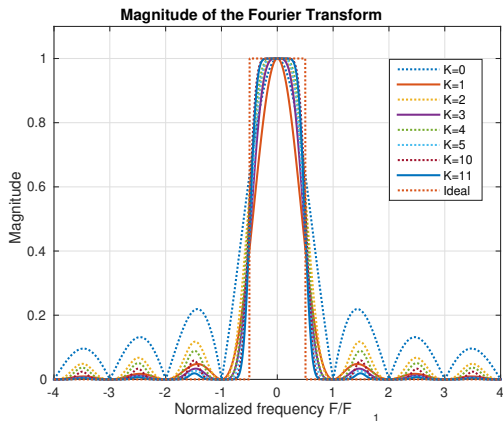
Figure 9: Magnitude of the O-spline Fourier transforms, $K = 0, 1, \ldots, 5$, 10 and 11.

Odd O-spline Spectra
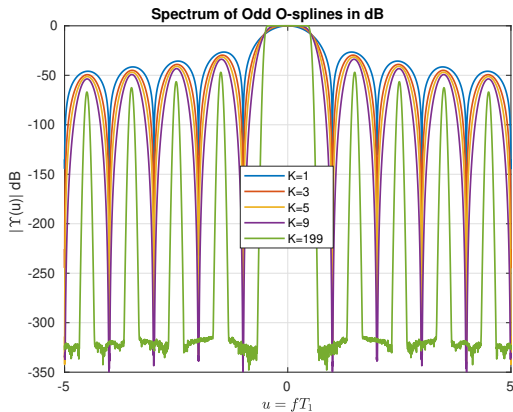
Figure 10: Spectra Odd O-splines, $K = 0, 1, \ldots, 9$, and 199.

Figure 11: Impulse and magnitude responses of the first differentiators,
$K = 0, 1, \ldots, 5, 10$ and 11.

Second Differentiators and their Spectra
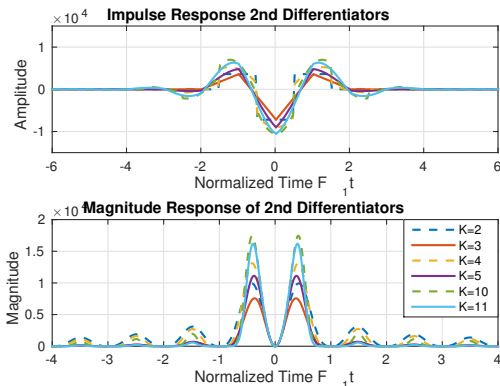
Figure 12: Impulse and magnitude responses of the second differentiators, $K = 0, 1, \ldots, 5$, 10 and 11.

Conclusions about O-splines

- Odd order O-splines are cardinal splines with compact support.
- They offer a ladder of function spaces very useful for multi-resolution analysis.
- They are maximally-flat differentiators that provide state sampling of signals.
- They allow us to estimate not only the signal, but also its instantaneous speed and acceleration.
- Used as bandpass filters, they provide not only the synchrophasor of a signal but also its derivatives, from which amplitude, phase, frequency and ROCOF are obtained.
- They are very useful to analyze modes in power oscillations, with better precision than the Prony method.
- Off course, they are efficient when the signal spectral density is located under the ideal gain of the filters.

Fast Taylor-Fourier Transform

We have:

$$\widehat{\xi}_K = \Omega_K^{-1}\widetilde{\Upsilon}_K^{-1}x$$

$$= \frac{1}{N}\begin{pmatrix} W_N^H & 0 & \ldots & 0 \\ 0 & W_N^H & \ldots & 0 \\ \vdots & \vdots & \ddots & \vdots \\ 0 & 0 & \ldots & W_N^H \end{pmatrix}\begin{pmatrix} \widetilde{Y}_1 & \widetilde{Y}_2 & \ldots & \widetilde{Y}_C \\ \overset{\centerdot}{\widetilde{Y}}_1 & \overset{\centerdot}{\widetilde{Y}}_2 & \ldots & \overset{\centerdot}{\widetilde{Y}}_C \\ \vdots & \vdots & \ddots & \vdots \\ \widetilde{\overset{(K)}{Y}}_1 & \widetilde{\overset{(K)}{Y}}_2 & \ldots & \widetilde{\overset{(K)}{Y}}_C \end{pmatrix}\begin{pmatrix} x_1 \\ x_2 \\ \vdots \\ x_C \end{pmatrix}$$

$$(30)$$

- The FTFT results by implementing the product $\widetilde{\Upsilon}_K^{-1}x$, and then multiplying by Ω_K^{-1}.
- Each row of the product $\widetilde{\Upsilon}_K^{-1}x$ is the cyclic addition of the Hadamard real product (.*) between the Ospline in that row and the signal x.
- Then, the Fourier operator produces the FFTs of the former cyclic additions.

Synthesis Equation

For any order K, and observation interval t, the synthesis equation is given by:

$$x(t) = \Upsilon_K \Omega_K \xi_k(\tau) \tag{31}$$

where τ is the estimation time instance, at the center of the observation interval t, and $\xi_k(\tau)$ contains the estimated Taylor-Fourier coefficients:

$$\xi_K(\tau) = \Omega_K^{-1} \widetilde{\Upsilon}_K^{-1} x(t) \tag{32}$$

For each K, the basis vector in Φ_K spans a complete space $V = \mathcal{R}^{(K+1)N}$, on the observation interval of length $(K+1)N$ cycles, since for any K we have:

$$x(t) = \Upsilon_K \Omega_K \Omega_K^{-1} \widetilde{\Upsilon}_K^{-1} x(t) = \Upsilon_K \widetilde{\Upsilon}_K^{-1} x(t) = x(t) \tag{33}$$

Instantaneous Synthesis Equation

On the other hand, the series of instantaneous Taylor-Fourier coefficients $\xi_h(t)$ constitute the analytic functions of the hth harmonic signals and their corresponding derivatives. For any harmonic h, we have the following instananeous reconstruction:

$$s_h(t) = a_h(t) \cdot \cos(\Phi_h(t)) = 2Re\{\xi_h(t)\} \tag{34}$$

$$\dot{s}_h(t) = 2Re\{\dot{\xi}_h(t)\} \tag{35}$$

$$\cdots \tag{36}$$

$$\overset{(K)}{s}(t) = 2Re\{\overset{(K)}{\xi}_h(t)\} \tag{37}$$

- In (32), each set of harmonic derivatives is channeled independently of the others.
- One FFT is needed *per* derivative harmonic set.
- Only 3 FFTs are needed to obtain the main three harmonic full sets.

Example: Amplitude modulated harmonic and its derivatives
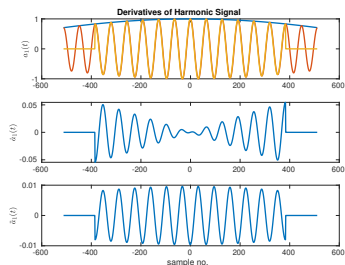
Figure 13: First three derivatives of amplitude modulated harmonic.

$$a_1(t) = A(t)\cos(2\pi F_1 t) \tag{38}$$

$$\dot{a}_1(t) = \dot{A}(t)\cos(2\pi F_1 t) - 2\pi F_1 A(t)\sin(2\pi F1t) \tag{39}$$

$$\ddot{a}_1(t) = [\ddot{A}(t) - 4\pi^2 F_1^2 A(t)]\cos(2\pi F_1 t) - 4\pi F_1 \dot{A}(t)\sin(2\pi F_1 t) \tag{40}$$
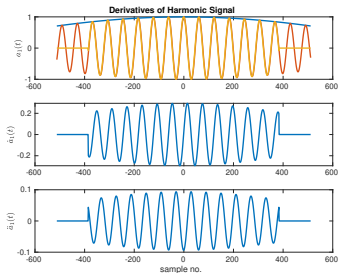
Figure 14: First three derivatives of amplitude and phase modulated harmonic.

$$a_1(t) = A(t)\cos(\Phi(t)) \tag{41}$$

$$\dot{a}_1(t) = \dot{A}(t)\cos(\Phi(t)) - A(t)\dot{\Phi}(t)\sin(\Phi(t)) \tag{42}$$

$$\ddot{a}_1(t) = [\ddot{A}(t) - A(t)\dot{\Phi}(t)^2]\cos(\Phi(t)) - [2\dot{A}(t)\dot{\Phi}(t) + A(t)\ddot{\Phi}(t)]\sin(\Phi(t)) \tag{43}$$

Conclusions FTFT

- Fast Taylor-Fourier transform can be calculated with one FFT for each derivative of the harmonic set.
- The evolution of the instantaneous Taylor-Fourier coefficients provides the analytic function of each harmonic derivative.
- 3 FFTs are needed to collect the first three derivatives of each harmonic
- From the analytic signals the amplitude and phase derivatives of the oscillations can be computated.
- The implications in coding of this transform need to be further investigated.

Analazing Power Oscillations[2]
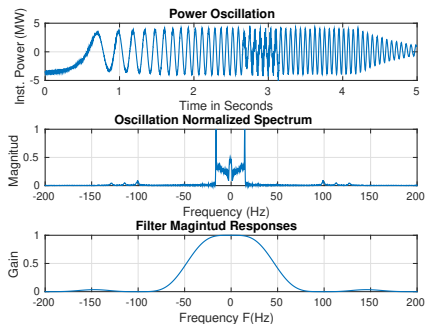
Figure 15: PO (top plot) and its spectrum (middle plot), and frequency response of splitting filters (at the bottom).

---

[2] J.A. de la O, "Analyzing Power Oscillating Signals with the O-splines of the Discrete Taylor-Fourier Transform", *IEEE Transactions on Power Systems*, vol. 33, no. 6, Nov. 2018, pp. 7087-7095.

Oscillation Spectrogram
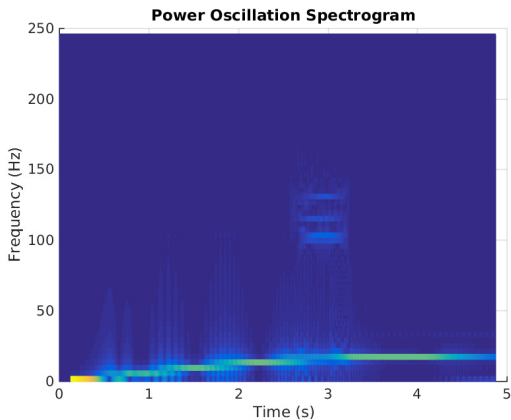
Figure 16: Spectrogram of the oscillation with varying frequency.

Estimated Angle and Frequency Modulations (Spectrogram)
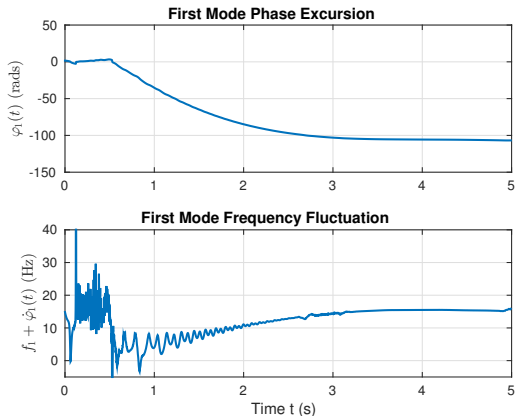
Figure 17: Estimated phase and frequency modulation (Spectrogram).
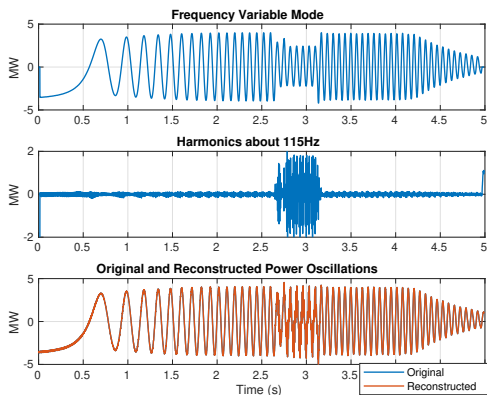
Figure 18: Frequency modulating mode (top plot) and harmonics about $115Hz$ (middle plot), with the original and reconstructed PO.

Co-authors in DTTFT Papers

Figure 19: Coauthors in DTTFT design or applications papers (Wendy Van Moer, Tom Van Acker).

(a) Mario Arrieta P.   (b) Alejandro Zamora

Figure 20

[3]J. A. de la O Serna, M. R. Arrieta Paternina, A. Zamora-Mendez, "Assessing Synchrophasor Estimates of an Event Captured by a Phasor Measurement Unit", *IEEE Transactions on Power Delivery*, IEEE Xplore Early Access

Synchrophasor Estimation from Real Signals

- Synchrophasor estimates can be evaluated with TVE only for the very few and lax benchmark signals of the Standard.

- This dependence prevents its application to power signals of real events.

- Our research problem is to quantify the erratic phasor estimates provided by a PMU from a real case in a power system.

- The solution of this problem is proposed for obtaining the synchrophasor of real signals.

- A nonic O-spline filter obtains phasor estimates asymptotically close to those obtained with an *ideal bandpass filter*.

- Once the synchrophasor is obtained, the accuracy of one or several PMUs can be assessed using the TVE.

- This solution opens the way to compare synchrophasor estimates of PMUs of different brands, when they process signals of the same power system event.
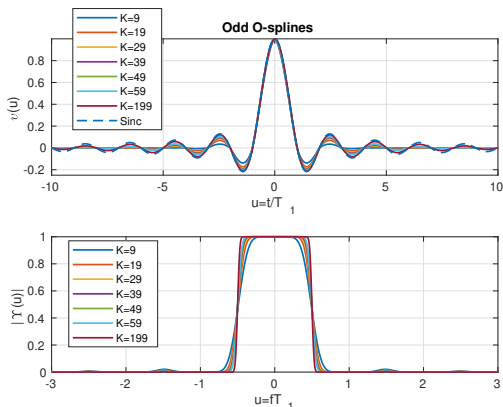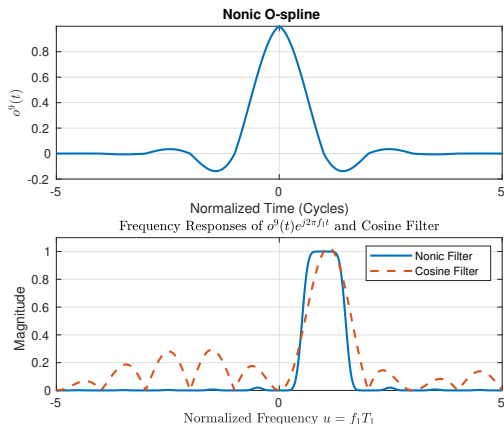
Figure 21: O-spline convergence to $Sinc(t)$, and $U(F)$.

Assesing PMU Measurements

Figure 22: Ten-cycle Nonic O-spline (top plot) used to extract the synchrophasor, and at the bottom its frequency response compared with that of the Cosine filter used in the PMU.
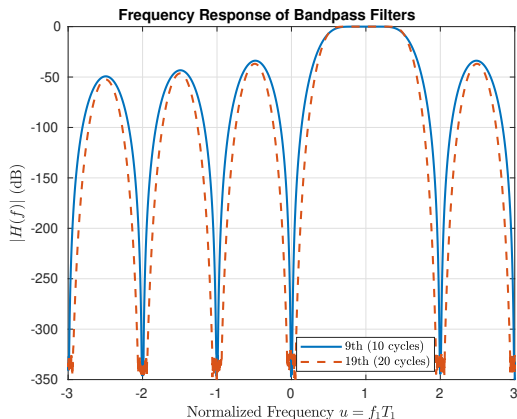
Figure 23: Nonic and decimononic bandpass filters frequency responses.

_____

[4]Distance very small between 9th and 19th O-spline synchrophasors. In a convergent Cauchy sequence, this indicates that their estimates have reached to the ideal synchrophasor.
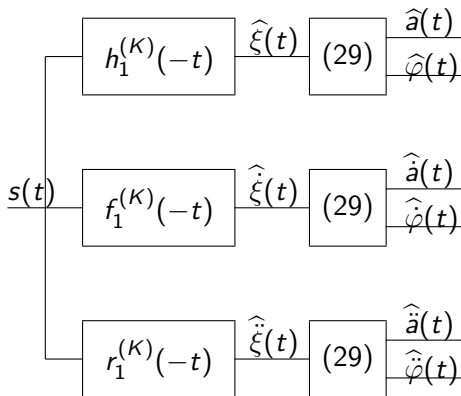
Figure 24: Flowchart of the proposed method.

Table 1: Steady State Compliance.

Case	Measurement	Standard Limit
$f_0 \pm 5$ Hz	$TVE = 2.185 \times 10^{-5}$ %	1%
	$|FE| = 0$ Hz	0.005 Hz
	$|RFE| = 5.128 \times 10^{-6}$ Hz/s	0.1 Hz/s
10 % Harmonic distortion up to 50th	$TVE = 2.5 \times 10^{-12}$ %	1 %
	$|FE| = 6 \times 10^{-15}$ Hz	0.025Hz
	$|RFE| = 1.5 \times 10^{-13}$ Hz/s	Limit Suspended
Out-of-Band	$TVE = 2.9933$ %	1.3 %
	$|FE| = 1.166 \times 10^{-05}$ Hz	0.01 Hz
	$|RFE| = 6.9919 \times 10^{-05}$ Hz/s	Limit Suspended

Table 2: Dynamic Compliance - Measurement Bandwidth.

Case	Measurement	Standard Limit
Amplitude Modulated	$TVE \leq 2.5 \times 10^{-6}$ %	3 %
	$|FE| \leq 1.95 \times 10^{-7}$ Hz	0.3 Hz
	$|RFE| < 7.357 \times 10^{-6}$ Hz/s	14 Hz/s
Phase Modulated	$TVE \leq 4.71 \times 10^{-5}$ %	3 %
	$|FE| \leq 6.92 \times 10^{-6}$ Hz	0.3 Hz
	$|RFE| < 1.65 \times 10^{-3}$ Hz/s	14 Hz/s.
Frequency Modulated	$TVE \leq 2 \times 10^{-5}$ %	1 %
	$|FE| \leq 1.627 \times 10^{-6}$ Hz	0.01 Hz
	$|RFE| < 5 \times 10^{-4}$ Hz/s	0.2 Hz/s

Dynamic Compliance - Step Responses.

Table 3: Dynamic Complience - Step Responses.

Case	Measurement	Standard Limit
Amplitude Step	Response time = 7.23 cycles	7 cycles
	delay time = 0 cycles	$\frac{1}{4}$ cycle
	Overshoot = 6.4 %	10 %
	Frequency response time = 6 cycles	14 cycles
	ROCOF response time = 6 cycles	14 cycles
Phase Step	Response time = 7.37 cycles	7 cycles
	delay time = 0 cycles	$\frac{1}{4}$ cycle
	Overshoot = 7.4 %	10 %
	Frequency response time = 6 cycles	14 cycles
	ROCOF response time = 8 cycles	14 cycles
Modulated Frequency	$TVE \leq 2 \times 10^{-5}$ %	1 %
	$|FE| \leq 1.627 \times 10^{-6}$ Hz	0.01 Hz
	$|RFE| < 5 \times 10^{-4}$ Hz/s	0.2 Hz/s
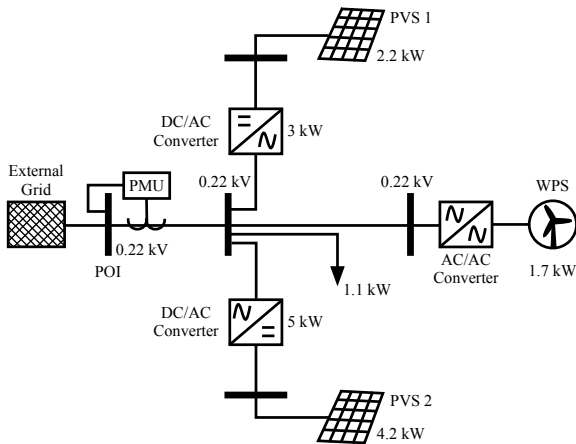
Figure 25: Topology of the low-voltage distributed generation system considered in this paper with two PVSs and one WPS interconnected to the grid.
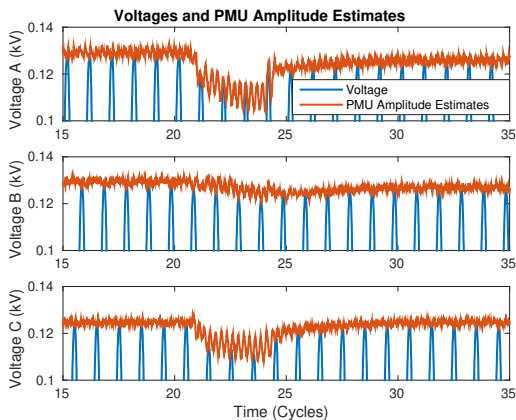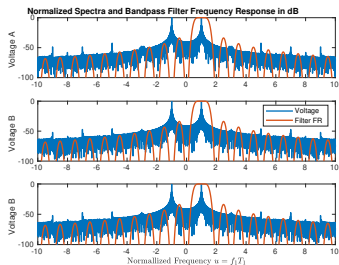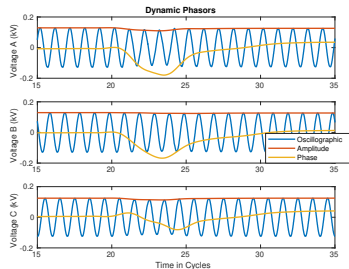
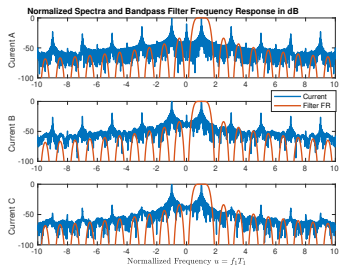Figure 26: Voltage waveforms with amplitude estimated by the PMU.
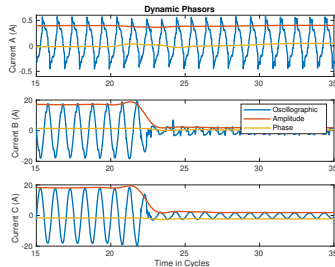
(a) Spectra and fundamental bandpass filter

(b) Dynamic Phasors.

Figure 27: Voltage spectra and nonic DTTFT filter frequency response. At the bottom, voltage oscillography and the corresponding synchrophasors.

Current Spectra

(a) Spectra and fundamental bandpass filter

(b) Dynamic Phasors.

Figure 28: Current spectra and nonic DTTFT filter frequency response. At the bottom, current oscillography and the corresponding synchrophasors (amplitude and phase).
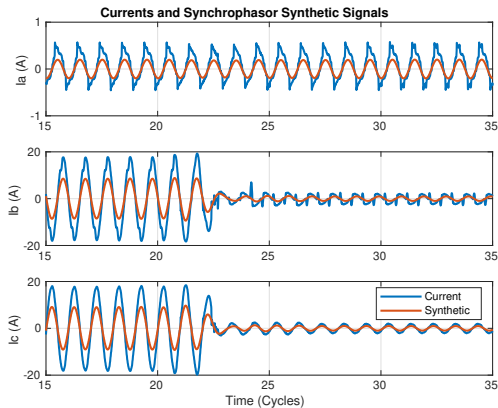
Figure 29: Currents and their synchrophasor synthetic signals.
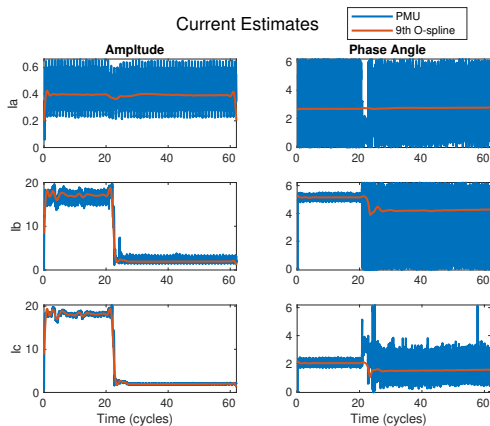
Current Phasor Estimates

Figure 30: Current phasor estimates. At the left column the amplitudes, and at the right column the corresponding phase angles.
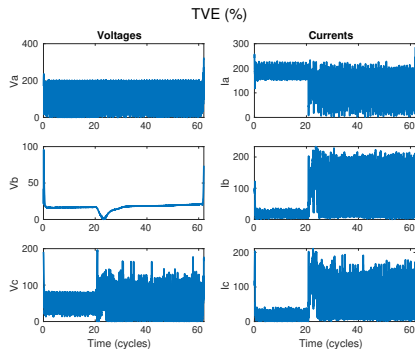
Figure 31: TVE of PMU Voltage (left), and current (right) estimates.
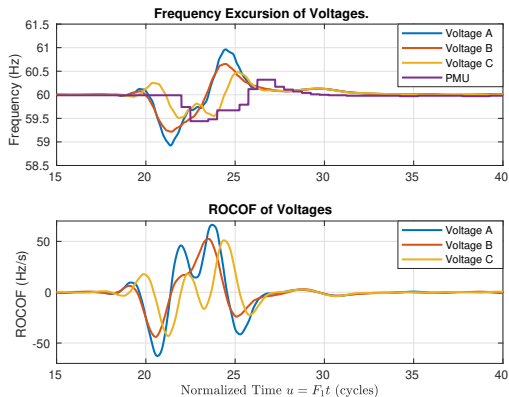
Figure 32: Frequency and ROCOF estimates from voltage channels obtained with the nonic O-spline first and second differentiators.

- Standards reflect the global *consensus* and *distilled wisdom* of many technical delegated experts.

- They provide instructions, guidelines, rules or definitions that are used to *design, manufacture, install, test & certify, maintain and repair electrical and electronic* devices and systems.

- They are essential for quality and risk management;

- Standards are always used by voluntary technical experts (and based on *international consensus*).

- They help researchers to understand the value of innovation and allow *manufacturers* to produce products of *consistent quality and performance*.

---

[5] Taken from: https://www.iec.ch/understanding-standards

Discussion II: Synchrophasor Standard
IEC/IEEE 60255-118-1

- Standards are not for promoting scientific *research*, it is the other way around.
- The O-spline performance shows that the standard limits are unduly lax.
- The standard prevents to test PMUs with real signals whose synchrophasors are unknown.
- TVE only takes into account amplitude and phase. A synthetic error including frequency and ROCOF is required.
- Out-of-Band test obliges to filter out important oscillations due to a low reportig rate.
- The standard allows noisy frequency and ROCOF estimates.

Conclusions PMUs Phasor Estimates

- The paper proposes a quantitative method to assess the estimation performance of PMUs using signals from the field, instead of only with the few benchmark signals of the Standard.
- Real signals contain realistic harmonics and real noisy conditions.
- The analyzed case exhibits very poor and erratic PMU estimates, with intolerable TVEs.
- This work opens up the possibility of employing the TVE to assess and compare the estimation performance of different PMUs at a control center, when they monitor the same disturbance.
- Application that was considered before as unthinkable and impossible.

Introduction to De la O Wavelets

- Wavelets are function orthogonal to cyclic time translations. With them perfect reconstruction can be achieved through the *Discrete Wavelet Transform* algorithm

- O-splines can be transformed into wavelets with the frequency compensation used by Battle-Lemarié to orthogonalize translated B-splines.

(a) Jaime Menéndez Álvarez

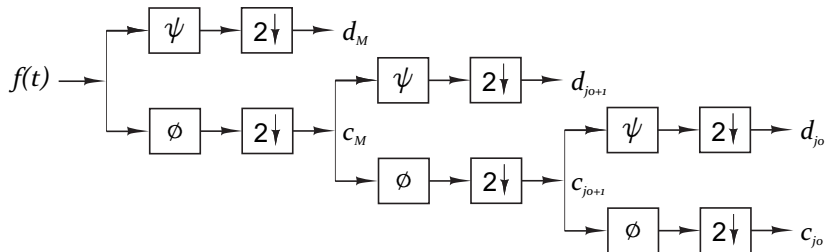(b) Gina Idárraga-Ospina

Figure 33: *Discrete Wavelet Transform* algorithm through low and high pass filter bank.
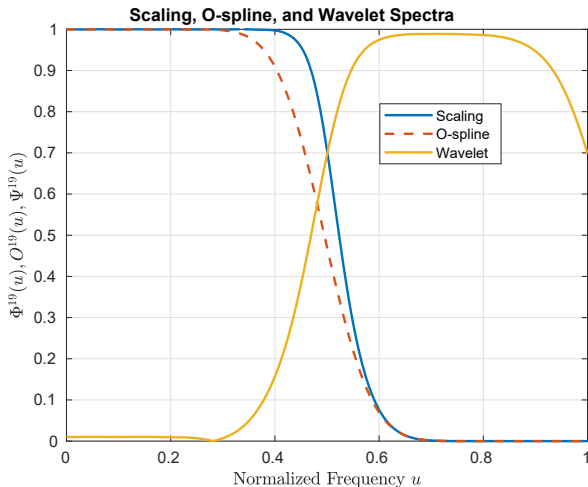
Figure 34: Spectra of decimononic scaling function, O-spline, and Wavelet functions.
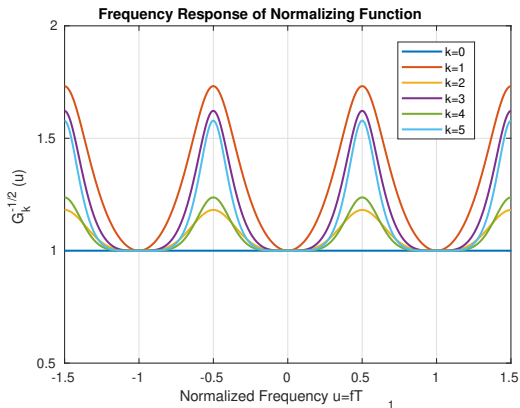
Frequency compensation function

Figure 35: Periodic normalizing function $1/\sqrt{G_k(u)}$.
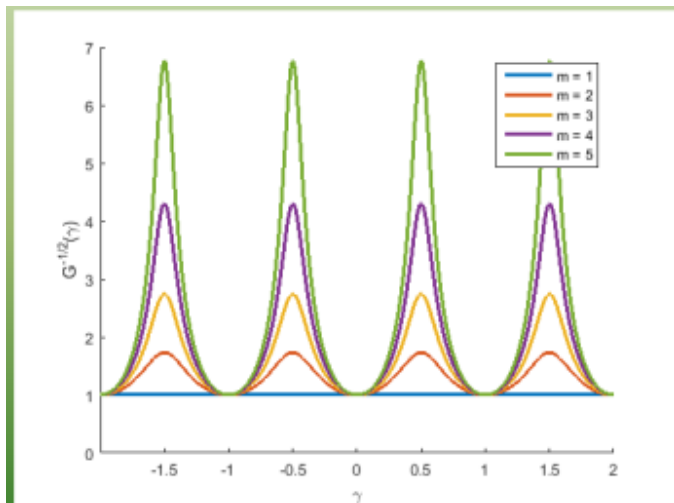
Battle-Lemarié Frequency Gain

Figure 36: Battle-Lemarié Compensation Gain for B-splines

Scalar and Wavelet Functions: Meyer and de la O nonic and decimononic.
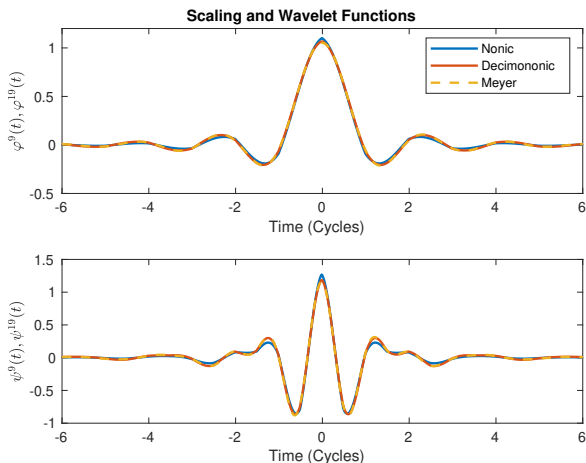

Figure 37: Scaling functions and Wavelets: Meyer and de la O nonic and decimononic.

de la O$^\infty$ and Bandlimited Scalar and Wavelet functions
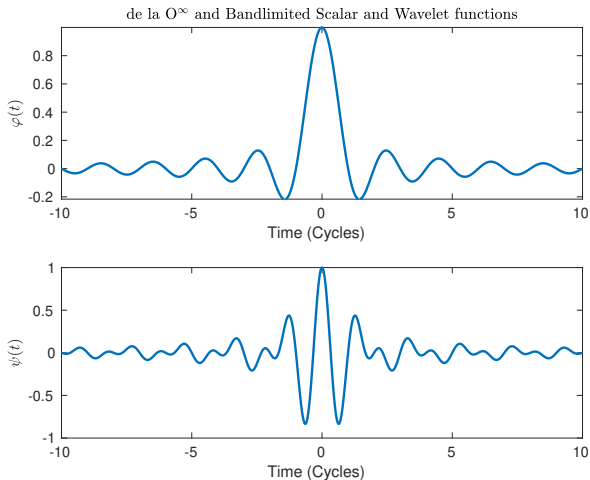
Figure 38: Scaling functions and Wavelets: Bandlimited and de la O$^\infty$.

Mathematicians involved in this work

- Johann Carl Friedrich **Gauss**, Augustin-Louis **Cauchy**
- Leonhard **Euler**
- Joseph **Fourier**
- Brook **Taylor**
- Gaspard Richard **de Prony**
- David **Hilbert**
- Marc Antoine **Parseval**, Friedrich Wilhelm **Bessel**, Brian Lewis **Butterworth**, Pafnuty **Chebyshev**
- Rudolf E. **Kalman**
- Yves **Meyer**, Guy A. **Battle**, Pierre Gilles **Lemarié**-**Rieusset**, Stéphan **Mallat**, Ingrid **Daubechys**, Jalena **Kovačević**, Martin **Vetterli**, David **Walnut**.

Future Paper on Dynamic Impedance

- Paper "Assessment of Harmonic Network Impedance through Transient Harmonic Signals" by Tom Van Acker
- Julia Package at GitHub:
  https://github.com/timmyfaraday/TFT.jl
- Main idea

$$\lim_{\Delta t \to 0} \frac{\Delta \overline{U}_{h,s}(t)}{\Delta t} = \overline{Z}_{h,s}^{\text{ntw}} \lim_{\Delta t \to 0} \frac{\Delta \overline{I}_{h,s}(t)}{\Delta t}, \quad \overline{U}_{h,s}^{(1)}(t) = \overline{Z}_{h,s}^{\text{ntw}} \overline{I}_{h,s}^{(1)}(t).$$

(a) Tom Van Acker, BASF, Belgium.

FTFT papers to come in Power Systems

1. Book Chapter: Power Quality Harmonic Monitoring by the O-splines-based Multiresolution Signal Decomposition
2. "Fast Taylor-Fourier Transform for Monitoring Modern Power Grids with Real-Time Dynamic" Harmonic Estimation
3. "Model-Free Inertia Estimation in Bulk Power Grids Through O-splines"
4. "Adaptive Discrimination Scheme for Transformer Differential Protection"
5. "O-splines-based Fixed-Frequency Integral Sliding-Mode Controller for PFC Rectifier"

Power System Concepts review due to FTFT

- Dynamic phasor
- Dynamic impedance
- Inertia estimation
- Harmonic packages through wavelets
- Power oscilation time-frequency analysis (and maybe spacial localization)
- Classification of power signals
- Dynamic Power Systems
- Automatic control algorithms
- Protection scheeme with transient information instead of static phasor scheme
- Power signals derivative interpretation.
- Dynamic states

Bibliografía

1. J. A. de la O Serna, "Dynamic Harmonic Analysis with FIR filters designed with O-splines", *IEEE Transactions on Circuits and Systems I: Regular Papers*, Vol.67, No.12, Dec. 2020, pp. 5092-5100.

2. J.A. de la O, "Analyzing Power Oscillating Signals with the O-splines of the Discrete Taylor-Fourier Transform", *IEEE Transactions on Power Systems*, vol. 33, no. 6, Nov. 2018, pp. 7087-7095.

3. J. A. de la O Serna, M. R. Arrieta Paternina, A. Zamora-Mendez, "Assessing Synchrophasor Estimates of an Event Captured by a Phasor Measurement Unit", *IEEE Transactions on Power Delivery*, IEEE Xplore Early Access: 26 Oct 2020.

Thanks.
jdelao@ieee.org
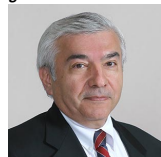
José Antonio de la O Serna(SM'03) received his Ph.D. degree from Telecom ParisTech, France, in 1982. In 1987 he joined the Ph.D. program in electrical engineering at the Autonomous University of Nuevo León (UANL), where he was a member of the Doctoral Committee. Currently he is research professor at the UANL, Monterrey, Mexico. He was also professor at Monterrey Institute of Technology from 1982 to 1986. From 1988 to 1993, he was with the Electrical Department at the Polytechnic School in Yaounde, Cameroon. Mr. de la O Serna is a member of the Mexican Research System.